




Article

Flood Inundation Modeling by Integrating HEC–RAS and Satellite Imagery: A Case Study of the Indus River Basin

Muhammad Adeel Afzal ¹, Sikandar Ali ^{1,2,*} , Aftab Nazeer ^{3,4,*}, Muhammad Imran Khan ¹, Muhammad Mohsin Waqas ⁵ , Rana Ammar Aslam ⁶, Muhammad Jehanzeb Masud Cheema ⁷ , Muhammad Nadeem ⁸, Naeem Saddique ¹, Muhammad Muzammil ^{1,9}  and Adnan Noor Shah ⁵ 

- ¹ Department of Irrigation and Drainage, Faculty of Agricultural Engineering and Technology, University of Agriculture, Faisalabad 38000, Pakistan
 - ² Agricultural Remote Sensing Lab, University of Agriculture, Faisalabad 38000, Pakistan
 - ³ Department of Water Management, Delft University of Technology, 2600 GA Delft, The Netherlands
 - ⁴ Department of Agricultural Engineering, Bahauddin Zakariya University, Multan 60800, Pakistan
 - ⁵ Department of Agricultural Engineering, Khwaja Fareed University of Engineering and Information Technology, Rahim Yar Khan 64200, Pakistan
 - ⁶ Department of Structures and Environmental Engineering, Faculty of Agricultural Engineering and Technology, University of Agriculture, Faisalabad 38000, Pakistan
 - ⁷ Department of Land and Water Conservation Engineering, Faculty of Agricultural Engineering and Technology, PMAS Arid Agriculture University, Rawalpindi 46000, Pakistan
 - ⁸ Department of Farm Machinery and Power, Faculty of Agricultural Engineering and Technology, University of Agriculture, Faisalabad 38000, Pakistan
 - ⁹ Institute for Landscape Ecology and Resources Management (ILR), Research Centre for BioSystems, Land Use and Nutrition (IFZ), Justus Liebig University, 35392 Giessen, Germany
- * Correspondence: sikandar_ali@uaf.edu.pk (S.A.); a.nazeer@tudelft.nl (A.N.); Tel.: +92-321-7659581 (S.A.); +31-649065653 (A.N.)



Citation: Afzal, M.A.; Ali, S.; Nazeer, A.; Khan, M.I.; Waqas, M.M.; Aslam, R.A.; Cheema, M.J.M.; Nadeem, M.; Saddique, N.; Muzammil, M.; et al. Flood Inundation Modeling by Integrating HEC–RAS and Satellite Imagery: A Case Study of the Indus River Basin. *Water* **2022**, *14*, 2984. <https://doi.org/10.3390/w14192984>

Academic Editor: Giuseppe T. Aronica

Received: 5 August 2022

Accepted: 16 September 2022

Published: 22 September 2022

Publisher's Note: MDPI stays neutral with regard to jurisdictional claims in published maps and institutional affiliations.



Copyright: © 2022 by the authors. Licensee MDPI, Basel, Switzerland. This article is an open access article distributed under the terms and conditions of the Creative Commons Attribution (CC BY) license (<https://creativecommons.org/licenses/by/4.0/>).

Abstract: Floods are brutal, catastrophic natural hazards which affect most human beings in terms of economy and life loss, especially in the large river basins worldwide. The Indus River basin is considered as one of the world's large river basins, comprising several major tributaries, and has experienced severe floods in its history. There is currently no proper early flood warning system for the Indus River which can help administrative authorities cope with such natural hazards. Hence, it is necessary to develop an early flood warning system by integrating a hydrodynamic model, in situ information, and satellite imagery. This study used Hydrologic Engineering Center–River Analysis System (HEC–RAS) to predict river dynamics under extreme flow events and inundation modeling. The calibration and validation of the HEC–RAS v5 model was performed for 2010 and 2015 flood events, respectively. Manning's roughness coefficient (n) values were extracted using the land use information of the rivers and floodplains. Multiple combinations of n values were used and optimized in the simulation process for the rivers and floodplains. The Landsat 5 Thematic Mapper (TM), Landsat 8 Operational Land Imager (OLI), Moderate Resolution Imaging Spectroradiometer (MODIS) MOD09A1, and MOD09GA products were used in the analysis. The Normalized Difference Water Index (NDWI), Modified NDWI1 (MNDWI1), and MNDWI2, were applied for the delineation of water bodies, and the output of all indices were blended to produce standard flood maps for accurate assessment of the HEC–RAS-based simulated flood extent. The optimized n values for rivers and floodplains were 0.055 and 0.06, respectively, with significant satisfaction of statistical parameters, indicating good agreement between simulated and observed flood extents. The HEC–RAS v5 model integrated with satellite imagery can be further used for early flood warnings in the central part of the Indus River basin.

Keywords: Indus River; HEC–RAS; inundation modeling; flood warning; MODIS; Landsat

1. Introduction

Human existence and survival on earth are vulnerable to innumerable damages caused by natural disasters [1,2]. Among these, floods are prominent as the most severe of disasters [3–5], affecting several million people annually [6], and claim more human lives compared with other brutal natural catastrophes worldwide [7,8]. River and coastal floods caused a total damage of about USD 46 trillion in 2010, which is expected to further project to USD 158 trillion in 2050 [9]. Floods have wrecked the global economy [10], and ruthlessly affected billions of people across the globe [11]. Floods also cause widespread damage to agriculture, transportation, environmental ecosystems, cultural heritage sites, and an overall disturbance to global economic activities [12,13]. Two primary types of flood damage are extensive damage and indistinct damage. Extensive damage can be assessed and translated into economic terms [14], while indistinct damage such as life loss cannot be assessed as financial losses [15]. Developing countries have suffered both extensive and indistinct damages, and compared with developed countries, suffer more per unit of their GDP due to the frequent and intensive floods under the changing climate [16], as they lack material and financial resources to mitigate the impacts [17].

Among developing countries, Pakistan has suffered a total flooded area of 616,598 km² [18], with an economic loss of about USD 38.171 billion, and lost 13,262 lives during the 25 major catastrophic floods in its history [19,20]. The huge economic and infrastructure losses are unavoidable in extreme floods due to the lack of dams, while the life loss is directly related to the lack of an early flood warning system, flood preparedness and management [21]. Pakistan receives water for its survival from the mighty Indus River basin and its tributaries [22]. The situation of the Indus basin is not only due to a lack of water storage facilities on the main Indus River, but also due to the lack of dams on its tributaries which also receive extreme flows [23,24]. Researchers are predicting more severe floods owing to climate variability [25], as the changing climate proves to be the leading cause of extreme floods worldwide [26–30]. In climate change scenarios, the timely warning of floods using conventional means is a challenge for better management, which has given rise to the scientific awareness of flood forecasting, preparedness and mitigation strategies among people [31,32].

Floods are also among the most commonly occurring disasters that cause geomorphologic flow channel deviations [33]. Unpredicted floods instigate physical effects on the flow paths and channel beds, i.e., changes in width, variations in bed elevations, flow path locus, flow behavior, and development of islands [15,34]. Sedimentation in heavy flood water further decreases the flood-carrying capacity of streams, hence increasing the possibility of bank overflows [35], and sedimentation usually happens in bars and flood-affected areas [36,37]. When the water level in the river exceeds the river's banks, water moves towards the floodplain, and the flows can be monitored and analyzed by computer simulations by performing flood inundation mapping. The aforementioned floods, associated damages, and management issues indicate that there is a need to properly accept the flood challenges and develop mitigation strategies [38–41], which can be helpful to minimize flood damage losses [42]. Therefore, hydrodynamic modeling and flood mapping of the rivers' basins are required to help the administrative authorities in the case of a flood emergency [43–46]. Hydrodynamic modeling of rivers and floodplains are performed to determine the possible flood extent and water depths that could be experienced due to a hydrological response, for different areas. All processes of hydrodynamic modeling require an accurate representation of the water channel, banks, flow paths and topography of the floodplain [47].

A hydrodynamic model illustrates the processes that occur throughout a flood event. There are usually two modeling approaches for the assessment of flood inundation and flood depths, namely, a one-dimensional approach and a two-dimensional assessment approach. In one-dimensional modeling, Saint Venant equations are utilized, and in the two-dimensional modeling approach, Saint Venant equations are used in two dimensions [48]. In one-dimensional modeling, the average values of water velocity and terrain cross-section

are used. The lateral flow of water, in the channel and floodplain, is not considered in one-dimension. Longitudinal flow is considered for the main channel and flood plains. A one-dimensional model is a suitable choice for assessing the direction of the flow path, but it does not consider lateral flow and the topography of cross-sections. On the other hand, in two-dimensional flood inundation mapping, the lateral and longitudinal flow of the channel and floodplains are considered. Two-dimensional models also represent the topography of the flow channel and floodplain [49]. Hydraulic modeling helps in timely warning, and evacuating, the possible affected areas downstream. Floodplain mapping requires online or offline applications [47], and offline hydraulic analysis is carried out using two-dimensional modeling in those areas where the geometry of the river flow is complex [50].

Both one-dimensional and two-dimensional analyses are carried out using different models combined with a geographical information system [51]. One-dimensional models show the flow through the river path and flooded area only in the horizontal direction. Two-dimensional models depend on incorporating the water height to acquire the average elevation of the water, and are analyzed by utilizing a suitable numerical methodology. One-dimensional modeling does not need comprehensive data, but two-dimensional modeling requires complex and detailed data of the river channel and floodplain [52]. Flow momentum, of the main channel and floodplain, is also included for steady and unsteady flow estimations in hydrodynamic modeling. The HEC–RAS v5 model has the capability of studying river dynamics under unsteady and steady state conditions [53]. HEC–RAS works in coordination with the flow data and results, as one of the productive flood inundation systems. Numerical exploration is considered one of the strategies available to carry out floodplain mapping. Therefore, in this study, critical methods were performed that helped evaluate the height of the water surface during overflow seasons. The well-known flood water levels were transformed into a topographic map, which outlined the regions of the floodplain that will be determined for flood forecasting [54].

A geographic information system (GIS) is an important tool to estimate the extent of floodwater and is also used for further analysis by creating maps to highlight damaged areas [55]. The integration of HEC-GeoRAS in ArcGIS software is a hybrid methodology for flood inundation mapping, for gathering, examining, and controlling spatial information [56]. Advanced floodplain mapping is obtained by consolidating all spatial and hydrological information [57]. The flood extent based on HEC–RAS simulations can be exported to ArcGIS software, and can be validated using satellite-based flood mapping [58–60] to further fine-tune the n values for the rivers and floodplain, and check the accuracy of the flood inundation modeling [61,62]. The mapping, monitoring, and variation of flood propagation can be addressed properly using a GIS [63]. The propagation of flood extent over floodplain mainly depends on the surface roughness of the rivers and floodplain [64,65]. The accurate assessment of Manning's roughness coefficient is of prime importance in the simulation of flood extent over the floodplain [66].

Inundation modeling for flood mapping over the Indus River basin is highly complicated and a big challenge; it is considered to be one of the largest basins on the globe [67], expanding from the higher mountains of the Himalaya to the Arabian Sea [68–70]. Researchers from different organizations of Pakistan are trying to develop an Early Flood Warning System using advanced hydrologic and hydrodynamic modeling of the rivers' basins. The United Nations Educational, Scientific and Cultural Organization is also trying to use different hydrological and hydrodynamic models in Pakistan and other parts of world to cope with the challenges of floods. The HEC–RAS v5 model is a popular inundation model and is being applied for inundation modeling and flood mapping worldwide [64,71–76]. The HEC–RAS model has been applied in different parts of the Indus River basin by researchers, such as in the Tori levee breach [77], Chashma–Taunsa reach [78], Kabul River reach [79], lower Indus River reach [80], and Hunza and Shyok rivers' reaches [81,82]. However, a few other models are also being applied by researchers in different parts of the Indus basin for flood mapping and inundation modeling [83–85]. The central parts of the Indus River

basin have still not been addressed; this area experiences severe floods, such as in 2010, which resulted in the flooding of a large area [86–88], depression and post-traumatic stress disorder [89–93], diseases and public health crisis [94–97], massive economic loss [21,98,99], environmental degradation [100–102], groundwater deterioration [103–105], and huge life loss [18,106,107]. The increased flood events and intensity, population growth, and climate change challenges have drawn the attention of scientists toward advanced spatiotemporal hydrodynamics modeling, instead of traditional flood modeling inundation. The present study focuses on advanced flood mapping by integrating an inundation model and satellite imagery in the central part of the Indus River basin using high resolution terrain information, soil type, and land use information. The calibrated and validated HEC–RAS v5 model can be further used for early flood warning in extreme future flood events.

2. Materials and Methods

2.1. Study Area

The Indus basin has a drainage area of more than 1,165,000 km², shared by China (10.7%), Afghanistan (6.7%), Pakistan (56%), and India (26.6%) [108]. The origin of the Indus River is Mansarovar Lake in the Tibetan Plateau. Before drainage into the Arabian Sea, it passes through Kashmir and Pakistan. The upper Indus basin is located in the range of 32.48° N and 67.33° E as presented in Figure 1, in the mountainous ranges of Karakoram, Hindu Kush, and Himalaya [109].

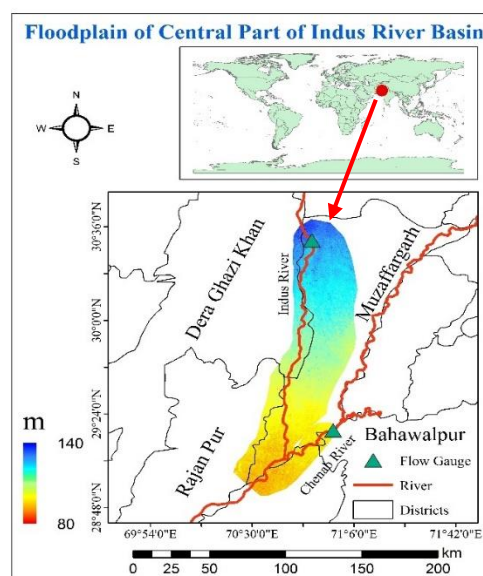


Figure 1. Elevation map of the Indus and Chenab rivers and their floodplains along with gauging stations.

These mountainous ranges comprise 11,000 glaciers [110], making it one of the most glaciated regions in the world, with a 22,000 km² surface area of glaciers [110]. The altitude varies from north to south and ranges between 200 m and 8500 m above sea level, with an average elevation of 3750 m above sea level. The study area is one of the major sources of fresh water for Pakistan. The study was conducted in the Indus River basin, from Taunsa Barrage to Kot Mithun, Punjab, a central part of the Indus River basin. The geographic boundary of the study area lies in 70.38°–71.10° E and 28.87°–30.64° N, while the elevation ranges from 80 to 140 m. Muzaffargarh, Dera Ghazi Khan, and Rajan Pur districts are subjected to frequent floods from the Indus and Chenab rivers. The Indus River basin has experienced high magnitude floods in 1956, 1973, 1976, 1992, 1994, 2010, 2015, and 2022, in its history [111]. The floods were of medium to high magnitude, which not only caused huge economic loss to the residents, but also claimed several lives. When the flood discharge reaches up to 17,000 m³/s, water starts overbank flow towards the floodplain of

the Indus River basin. When the flood discharge reaches up to 14,000 m³/s, water starts to overbank flow towards its floodplain. The Chenab River diverts water into the lower reach of the Indus River, which increases the flood magnitude of the Indus River and causes significant damage downstream.

2.2. Datasets Used in the Study

Inundation modeling through hydrodynamic simulation requires detailed and finer resolution information regarding soil type, land use, and topography [112–115]. Due to the lack of availability of cloud-free Landsat images, the daily MOD09GA product, as presented in Table 1, was used for land use classification of the study area. The normalized difference vegetation index (NDVI) initially proposed by [116], as presented in Equation (1), was used for land use classification through supervised classification. The land use information was further used to assign the n values, representing resistance to the flow of water over the floodplain, with the help of literature [117,118]. Detailed soil type information drawn from the Harmonized World Soil Database v 1.2 with a spatial resolution of 1 km [119] was used in the inundation modeling, which also plays an important role in hydrologic and hydrodynamic modeling of rivers' basins [120,121].

$$NDVI = \frac{NIR - RED}{NIR + RED} \quad (1)$$

2.3. Numerical Simulation in the HEC–RAS Model

The two-dimensional inundation modeling needs detailed topographic information of rivers and floodplains [52] to simulate flood propagation over the floodplain, systematically [122,123]. In this study, the radiometrically terrain corrected (RTC) digital elevation model (DEM) [124,125] of phased array type L-band synthetic aperture radar (PALSAR), mounted on the Advanced Land Observing Satellite-1, was used with a spatial resolution of 12.5 m. The DEM was further converted to a continuous surface triangulated irregular network (TIN) to extract rivers' cross sections and floodplain geometry. The TIN was further processed in HEC-GeoRAS in ArcGIS software for the extraction of rivers' parameters such as flow paths, rivers' banks, cross sections, etc. All the parameters were then exported from HEC-GeoRAS to be used in the HEC–RAS model. All the values of Manning's roughness coefficient were applied to each cross section. The inflow hydrograph at both flow gauges was used as boundary conditions to assign the flow to cells covering the complete river width at 1st cross-sections of the Indus and Chenab rivers. HEC–RAS v5 performs inundation simulation by solving two-dimensional Saint-Venant / diffusive wave equations [126,127]:

$$\frac{\partial \zeta}{\partial t} + \frac{\partial p}{\partial x} + \frac{\partial q}{\partial x} = 0 \quad (2)$$

$$\frac{\partial p}{\partial t} + \frac{\partial}{\partial x} \left(\frac{p^2}{h} \right) + \frac{\partial}{\partial y} \left(\frac{pq}{h} \right) = - \frac{n^2 pg \sqrt{p^2 + q^2}}{h^2} - gh \frac{\partial \zeta}{\partial x} + pf + \frac{\partial}{\partial x} (h\tau_{xx}) + \frac{\partial}{\partial y} (h\tau_{xy}) \quad (3)$$

$$\frac{\partial q}{\partial t} + \frac{\partial}{\partial y} \left(\frac{q^2}{h} \right) + \frac{\partial}{\partial x} \left(\frac{pq}{h} \right) = - \frac{n^2 qg \sqrt{p^2 + q^2}}{h^2} - gh \frac{\partial \zeta}{\partial x} + qf + \frac{\partial}{\partial y} (h\tau_{yy}) + \frac{\partial}{\partial x} (h\tau_{xy}) \quad (4)$$

where h is the depth of water (m), g is the acceleration due to the gravity (m s^{−2}), p and q are the specific flow (m² s^{−1}) in cartesian directions, n is the Manning resistance, ζ is the surface elevation (m), ρ is the density of water (kg m^{−3}), f is Coriolis (s^{−1}), and τ_{xx} , τ_{yy} and τ_{xy} are components of effective shear stress [127]. The initial terms of the Saint Venant Equations (3) and (4) were ignored for the diffusive wave equations. Both equations were applied with all possible combinations of n values for rivers (main channels) and floodplains, for simulation purposes.

2.4. Satellite-Based Flood Extent Mapping

The satellite datasets used for water bodies delineation in the study are also presented in Table 1. The geographic projection of MODIS and Landsat was transformed into a universal transverse Mercator projection. The NDWI equation, initially proposed by [128], was applied as presented below:

$$\text{NDWI} = \frac{\text{Green} - \text{NIR}}{\text{Green} + \text{NIR}} \quad (5)$$

Flood water contains a higher amount of sediments, therefore, a different modified NDWI (MNDWI) equation, initially proposed by [129], was also needed for flood mapping. MNDWI and MNDWI2 have also been used for flood mapping by researchers [130–132], as described below:

$$\text{MNDWI 1} = \frac{\text{Green} - \text{SWIR 1}}{\text{Green} + \text{SWIR 1}} \quad (6)$$

$$\text{MNDWI 2} = \frac{\text{Green} - \text{SWIR 2}}{\text{Green} + \text{SWIR 2}} \quad (7)$$

The details and standard referenced (literature-based) threshold values of NDWI, MNDWI 1, and MNDWI 2 used for flood mapping are described in Table 1. The theoretical consideration of threshold indicates flood cells with a value greater than 0 [133]; however, this threshold value of 0 is not practical in all extreme cases [134,135]. By considering the characteristics of water, an adjustment in threshold values is needed according to local conditions [130,136], therefore, the literature-based thresholds were used for the satellite-based flood mapping. All algorithms of water body delineation were applied, and a union method was applied to produce a blended observed flood extent for comparing the HEC–RAS-based simulated flood extent.

Table 1. Satellite datasets and threshold values of NDWI, MNDWI 1, and MNDWI 2.

Satellite Datasets	Method	Threshold Values	References
Landsat 5 TM	NDWI (2,4)	0.234, 0.205	[137,138]
	MNDWI 1 (2,5)	0.35, 0.45, 0.33	[135,137,139]
Landsat 8 OLI	NDWI (3,5)	0.113, 0.09	[137,139]
	MNDWI 1 (3,6)	0.286, 0.33,	[139–141]
	MNDWI 2 (3,7)	0.25–0.31 0.462	[140]
MODIS (MOD09GA/MOD09A1)	NDWI (4,2)	0.0	[142]
	MNDWI 1 (4,6)	0.44, 0.34	[143,144]

Note: The satellite captures of floods are presented as supplementary figures (Figures S1 and S2).

2.5. Calibration and Validation of HEC–RAS Model

The calibration and validation of the HEC_RAS v5 model were performed for 2010 and 2015 flood events, respectively. Flow hydrographs were used for the simulation process for both calibration and validation periods. The flow hydrographs had a peak flow of 27,184 and 17,124 m³/s on 2 August 2010, and 5 August 2015 at Taunsa Barrage, respectively. Approximately 950 and 3398 m³/s of flood water was diverted from the Chenab River into the lower reach of the Indus River. Daily MOD09GA (2 August 2010), 8-day MOD09A1 (5 August 2010), and Landsat 5 TM (12 August 2010) were used to delineate the flood extent for 2010. The daily MOD09GA (6 August 2015), 8-day MOD09A1 (13 August 2015), and Landsat 8 OLI (10 August 2015) were used for delineation of the flood extent for 2015. The n values were optimized in the simulation process by comparing the simulated and observed flood extents for both 2010 and 2015. The river routing accuracy was assessed by comparing the simulated and observed magnitudes and times of peak flows at the barrages downstream.

2.6. Accuracy Assessment of HEC–RAS Model

An uncertainty analysis is necessary in flood inundation modeling, for accuracy assessment [145]. The simulated flood cells were compared with the observed flood cells obtained from satellite imagery, for accuracy assessment of the inundation modeling. The accuracy of the simulation was tested using F1 and F2 indicators recommended by [146]:

$$F1 = \frac{A}{A + B + C} \quad (8)$$

$$F2 = \frac{A - B}{A + B + C} \quad (9)$$

The Sørensen–Dice coefficient, also known as Dice similarity coefficient (DSC), is the quotient of similarity, and was also used to check the similarity between the simulated and observed flood areas.

$$DSC = \frac{2A}{2A + B + C} \quad (10)$$

The Jaccard distance (JD) was also used to measure dissimilarity between simulated flood areas and satellite-based (observed) flood areas.

$$JD = \frac{(A + B + C) - A}{A + B + C} \quad (11)$$

where, A is the accurately simulated flooded area (km²) in the satellite imagery, B is the simulated flood area (km²) which is not present (observed) in the satellite imagery, and C is the area (km²) which is not simulated as flood but present (observed) as a flood area in the satellite imagery. The JD ranges from 0 to ∞, and values close to 0 indicate less dissimilarity between simulated and observed flood areas. The F1, F2, and DSC values range from 0 to 1, −1 to 1, and 0 to 1, respectively, where the values close to 1 indicate the best agreement between simulated and the observed flood areas.

3. Results

3.1. Land Use of the Study Area

The major land uses of the floodplains include the production of cotton, rice, sugarcane, maize, and other fodders. The overall accuracy of the land use map of 2010 and 2015, was 64.06 and 61.64%, with 66 and 73 sampling points, respectively. The n values for floodplains against land use information used in the HEC–RAS model are presented in Figure 2. The estimation of n values was mainly dependent on the remote-sensing-based land use information of the floodplains. Propagation of the flood extent in inundation models mainly depends upon the surface roughness offered by the features of the floodplains.

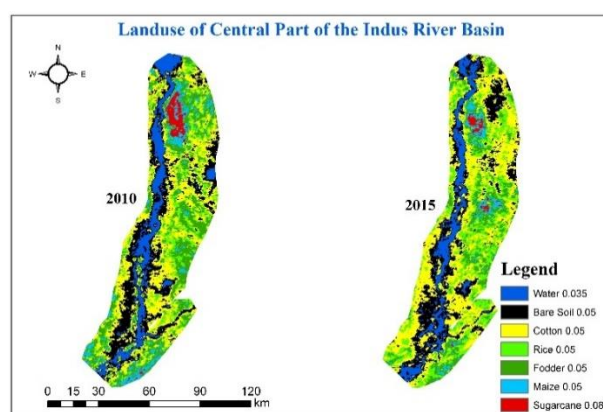


Figure 2. Land use information of floodplains for 2010 and 2015, developed using the MOD09GA product.

3.2. Performance Evaluation of HEC–RAS Model

Flood inundation simulation was performed for the 2010 flood against the input hydrograph at the very first HEC_RAS station of the study area. The simulation was carried out by assigning n values for the floodplains and the main channels (Indus River and its tributary, the Chenab River). The floodplains' and main channels' n values varied from 0.3 to 0.7 for simulation purposes, as presented in Table 2. The simulation performance of the HEC–RAS model for the calibration period indicated that the simulated flood area was increased by the increasing n values of the main rivers and floodplains, while the effect of the n value of the main channels was dominant. It is also evident from parameter A in Table 2 that the small increase in n value of the main channel caused a higher increase in the simulated flood extent, while increasing more floodplains' n values caused a small increase in the simulated flood extent. The observed flood area from the blended satellite-based flood extent was 5038 km². The lowest correctly simulated flood extent was recorded as 3626 km² with an n value of 0.03 for the main channels and floodplains. The highest correctly simulated flood extent was recorded as 4461 km² with n values of 0.055 to 0.07, and 0.06 to 0.07, for main channels and floodplains, respectively. The JD values indicated that the dissimilarities were smaller throughout the simulation process. The highest value of JD was 0.33 at a few smaller combinations of n values of main channels and floodplains, while the lowest value of JD was 0.23, which corresponded to the n values of 0.055 and 0.06 for the main channels and floodplains, respectively. It is also evident from Table 1 that the decrease in JD was higher with a smaller increase in n values of the main channels, while the decrease in JD was smaller even with a large increase in n value of the floodplains. The lowest values of F1, F2, and DSC corresponded to the lower n values of the floodplains and main channels. The highest values (nearest to 1) of F1, F2, and DSC, were 0.77, 0.64, and 0.87, which corresponded to the n values of 0.055 and 0.06, for main channels and floodplains, respectively. Higher values of F1 and F2 for inundation modeling were demonstrated by the researchers [147].

The numerical simulation of 2D diffusive wave equations to predict simulated flood cells were compared with the observed flood extents, as presented in Figure 3a,b. There was a good relationship between the simulated and observed flood extents near the river and in the lower part of the study area. There were some dissimilarities in the simulated and observed flood extents on the floodplains at the left bank of the river. It is evident from Figure 3a that there was a water depth of less than 3 m in most parts of the study area, while there were some areas where the water depth ranged from 3 to 4.5 m. The most difficult/problematic situation was in region of Rajan Pur, and the upper parts of Rahimyar Khan and Muzaffargarh districts, where water depth ranged from 3 to 6 m.

The simulation started with an input hydrograph at the first station for the validation period 2015, and the results are presented in Table 3. The satellite-based (observed) flood extent was 3302 km², and the lowest and highest correctly simulated flood extents were recorded as 2472 and 2996 km², respectively, with the same corresponding n value combinations of main channels and floodplains. The lowest values of F1, F2, and DSC were 0.71, 0.66, and 0.86, respectively, which also corresponded to the lower n values of floodplains and main channels and calibration period. The highest values (nearest to 1) of F1, F2, and DSC, were 0.81, 0.69, and 0.89, which also corresponded to n values of 0.06, for the main channels and floodplains. The higher values (close to 1) of F1, F2, and DSC indicated good validation results. The highest value of JD was 0.29 at a few smaller combinations of n values of main channels and floodplains, while the lowest value of JD was 0.19, which corresponded to the n values of 0.06 for the main channel and floodplains. The validation results were closely related to the calibration results; it is evident from Table 1 that the decrease in JD was also higher with a slight increase in the n values of the main channels. In contrast, the decrease in JD was smaller even with a large increase in the n values of the floodplains.

Table 2. Combinations of Manning’s roughness coefficient (n) values of floodplains and main channels for simulation during the calibration period 2010.

Parameter	Floodplain n	Main Channels (Rivers) n								
		0.03	0.035	0.04	0.045	0.05	0.055	0.06	0.065	0.07
A	0.03	3626	3716	3878	4029	4129	4167	4172	4172	4172
	0.04	3699	3745	3955	4108	4138	4159	4165	4165	4165
	0.05	3727	3809	3992	4148	4253	4291	4329	4329	4329
	0.06	3817	3886	4034	4217	4329	4461	4461	4461	4461
	0.07	3847	3963	4087	4265	4388	4461	4461	4461	4461
B	0.03	325	412	438	512	496	588	601	601	601
	0.04	447	511	541	601	638	622	624	624	624
	0.05	487	539	561	649	678	699	701	701	701
	0.06	512	586	635	697	714	758	816	816	816
	0.07	529	629	667	758	801	808	816	816	816
C	0.03	1412	1322	1160	1009	909	871	866	866	866
	0.04	1339	1293	1083	930	900	879	873	873	873
	0.05	1311	1229	1046	890	785	747	709	709	709
	0.06	1221	1152	1004	821	709	577	577	577	577
	0.07	1191	1075	951	773	650	577	577	577	577
F1	0.03	0.68	0.68	0.71	0.73	0.75	0.74	0.74	0.74	0.74
	0.04	0.67	0.67	0.71	0.73	0.73	0.73	0.74	0.74	0.74
	0.05	0.67	0.69	0.72	0.73	0.75	0.76	0.76	0.76	0.76
	0.06	0.69	0.70	0.71	0.74	0.76	0.77	0.76	0.76	0.76
	0.07	0.69	0.70	0.72	0.74	0.75	0.76	0.76	0.76	0.76
F2	0.03	0.62	0.61	0.63	0.63	0.66	0.64	0.63	0.63	0.63
	0.04	0.59	0.58	0.61	0.62	0.62	0.62	0.63	0.63	0.63
	0.05	0.59	0.59	0.61	0.62	0.63	0.63	0.63	0.63	0.63
	0.06	0.60	0.59	0.60	0.61	0.63	0.64	0.62	0.62	0.62
	0.07	0.60	0.59	0.60	0.61	0.61	0.62	0.62	0.62	0.62
DSC	0.03	0.81	0.81	0.83	0.84	0.85	0.85	0.85	0.85	0.85
	0.04	0.81	0.81	0.83	0.84	0.84	0.85	0.85	0.85	0.85
	0.05	0.81	0.81	0.83	0.84	0.85	0.86	0.86	0.86	0.86
	0.06	0.81	0.82	0.83	0.85	0.86	0.87	0.86	0.86	0.86
	0.07	0.82	0.82	0.83	0.85	0.86	0.87	0.86	0.86	0.86
JD	0.03	0.32	0.32	0.29	0.27	0.25	0.26	0.26	0.26	0.26
	0.04	0.33	0.33	0.29	0.27	0.27	0.27	0.26	0.26	0.26
	0.05	0.33	0.32	0.29	0.27	0.26	0.25	0.25	0.25	0.25
	0.06	0.31	0.31	0.29	0.26	0.25	0.23	0.24	0.24	0.24
	0.07	0.31	0.30	0.28	0.26	0.25	0.24	0.24	0.24	0.24

Table 3. Combinations of Manning’s roughness coefficient (n) values of floodplains and main channels for simulation during the validation period 2015.

Parameter	Floodplain n	Main Channels (Rivers) n								
		0.03	0.035	0.04	0.045	0.05	0.055	0.06	0.065	0.07
A	0.03	2472	2584	2628	2653	2715	2766	2791	2791	2791
	0.04	2585	2643	2679	2721	2773	2816	2828	2828	2828
	0.05	2642	2666	2757	2768	2809	2866	2907	2907	2907
	0.06	2709	2761	2804	2817	2848	2955	2996	2996	2996
	0.07	2751	2816	2862	2885	2909	2979	2996	2996	2996
B	0.03	178	197	215	239	269	305	321	321	321
	0.04	191	210	243	296	325	366	406	406	406
	0.05	212	247	281	313	347	394	416	416	416
	0.06	248	286	335	368	386	416	416	416	416
	0.07	279	323	347	381	402	426	446	446	446
C	0.03	830	718	674	649	587	536	511	511	511
	0.04	717	659	623	581	529	486	474	474	474
	0.05	660	636	545	534	493	436	395	395	395
	0.06	593	541	498	485	454	347	306	306	306
	0.07	551	486	440	417	393	323	306	306	306
F1	0.03	0.71	0.74	0.75	0.75	0.76	0.77	0.77	0.77	0.77
	0.04	0.74	0.75	0.76	0.76	0.76	0.77	0.76	0.76	0.76
	0.05	0.75	0.76	0.77	0.77	0.77	0.78	0.79	0.79	0.79
	0.06	0.76	0.77	0.77	0.77	0.78	0.80	0.81	0.81	0.81
	0.07	0.77	0.78	0.78	0.78	0.79	0.80	0.80	0.80	0.80
F2	0.03	0.66	0.68	0.69	0.68	0.68	0.68	0.68	0.68	0.68
	0.04	0.69	0.69	0.69	0.67	0.67	0.67	0.65	0.65	0.65
	0.05	0.69	0.68	0.69	0.68	0.67	0.67	0.67	0.67	0.67
	0.06	0.69	0.69	0.68	0.67	0.67	0.68	0.69	0.69	0.69
	0.07	0.69	0.69	0.69	0.68	0.68	0.68	0.68	0.68	0.68
DSC	0.03	0.83	0.85	0.86	0.86	0.86	0.87	0.87	0.87	0.87
	0.04	0.85	0.86	0.86	0.86	0.87	0.87	0.87	0.87	0.87
	0.05	0.86	0.86	0.87	0.87	0.87	0.87	0.88	0.88	0.88
	0.06	0.87	0.87	0.87	0.87	0.87	0.89	0.89	0.89	0.89
	0.07	0.87	0.87	0.88	0.88	0.88	0.89	0.89	0.89	0.89
JD	0.03	0.29	0.26	0.25	0.25	0.24	0.23	0.23	0.23	0.23
	0.04	0.26	0.25	0.24	0.24	0.24	0.23	0.24	0.24	0.24
	0.05	0.25	0.25	0.23	0.23	0.23	0.22	0.22	0.22	0.22
	0.06	0.24	0.23	0.23	0.23	0.23	0.21	0.19	0.19	0.19
	0.07	0.23	0.22	0.22	0.22	0.21	0.20	0.20	0.20	0.20

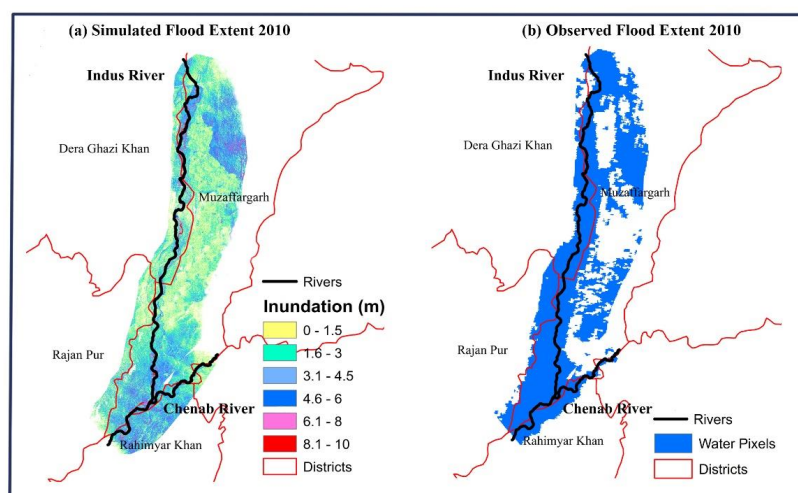


Figure 3. (a,b) HEC–RAS-based simulated and satellite-based flood area for the 2010 flood.

The comparison of simulated and observed flood areas is presented in Figure 4a,b. As discharge was not much higher than the calibration period, the simulated and observed flood extents were smaller. There was a similarity in the observed and simulated flood extents in almost all parts of the study area, except the upper parts of the Indus and Chenab rivers' confluence, where the modeled flood area was more, and the observed flood area was less. The water depth in most parts of the study area was less than 3 m, while some areas received a water depth of 3.5–4.5 m. Similarly, for the calibration period, similar parts of the study area received a flood depth of more than 4.5 m, but the extent of those areas was less than the calibration period. The slightly lower values of F1, F2, and DSC, and slightly higher values of DJ for calibration and validation period, were closely related to the resolution of topographic information which was used in the study. For the calibration period, the coarser resolution MOD09GA product was available the very next day, but Landsat 5 TM was only available 10 days after the flood date. For the validation period 2015, Landsat 8 OLI was available 5 days after the flood date and MOD09GA was available the very next day after the flood date. The MOD09A1 product was available after 3 and 8 days, for the calibration and validation period, respectively. The delay in high resolution Landsat images caused the misclassification of flood cells used in calibration and validation periods. The misclassification of flood cells, along with other topographic, hydrometeorological and roughness factors, caused a slight reduction in F1, F2, and DSC for the calibration and validation periods.

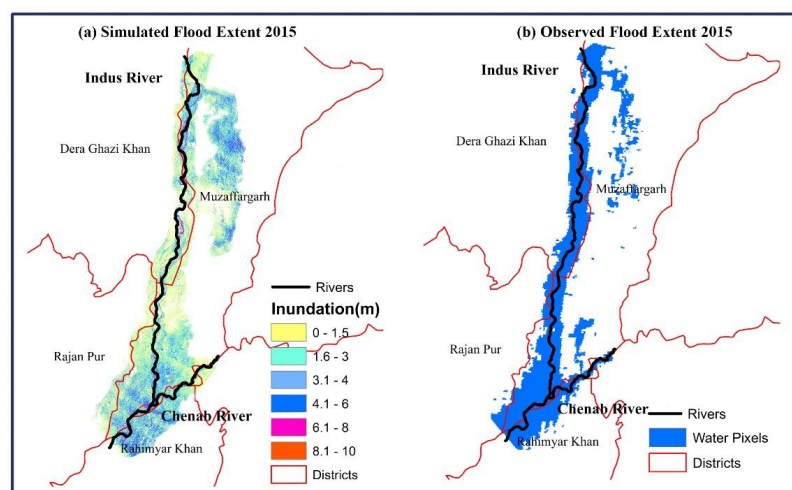


Figure 4. (a,b) HEC–RAS-based simulated and satellite-based flood area for the 2015 flood.

4. Discussion

The slightly lower values of F1, F2, and DSC, and slightly higher values of DJ were due to several errors associated with the satellite imagery and simulation in HEC-RAS. The overall accuracy of the land use map for 2010 and 2015 was not higher. The reason may be due to the small number of sampling data and poor resolution of the MOD09GA product, wavelength, polarization, and incident angle. The n values of the floodplain and main channels, estimated using land use information, play a key role in the propagation of floods over the floodplain, by offering resistance to the flood propagation. The n values within the floodplains are not a fixed quantity; however, they are a scale-dependent parameter representing all energy losses, which may also include drag force due to the presence of bridges. This highlights the significance of land use in hydrodynamic modeling, as dense vegetation surface offers significant friction to floodwater, and the least friction is offered by unvegetated areas [148]. Hence, the spatial variation of n values corresponding to the estimated land use information in the floodplains directly affects the parametrization of n values, and the accuracy of inundation modeling [49,149]. The accuracies of flood inundation modeling, water depth and flood extent are directly influenced by TIN, which is developed using topographic information of the rivers and floodplains [150–152]. This highlights the significance of river cross sections and floodplain geometry, which are mainly dependent on the TIN, indicating that the use of RTC DEM can improve the accuracy of hydrodynamic modeling. However, the accuracy of flood inundation simulation modeling can be further enhanced by using higher resolution topographic information of the study area [153]. It was also observed, during the simulation, that propagation of the flood extent was more dependent on the water surface elevation in the main channel, compared with the floodplain surface roughness, which was also observed by other researchers [147]. The wetness and dryness patterns of the floodplains play a key role in the propagation of flood extent [154], as the simulated flood extent and its propagation was directly related to parametrized n values, soil moisture conditions, in situ rainfall, and wind conditions of the floodplains [147]. These scientific findings revealed that the use of in situ or satellite-based soil moisture, rainfall, and wind conditions can be further integrated with hydrodynamic models to increase the overall accuracy of inundation modeling.

An accurate assessment of flood extent can be obtained from in situ observation and field surveys, which is not possible during the flood event. Satellite imagery is the only alternative source for flood mapping during and after the hazard [155–157], which can be utilized as a standard product for flood inundation modeling [158]. The flood inundation models have been calibrated [159] and validated [160] by the researchers with SAR satellite imagery. The time delay between the flood date and satellite imagery acquisition is one of the major factors associated with slightly lower accuracy of flood inundation modeling [161]. The flood extent delineation from satellite imagery is also sensitive to the date of acquisition, wavelengths of sensors, polarization, incident angle, and prevailing atmospheric conditions [147]. There is a need to further improve the accuracy of flood inundation modeling in the central part of the Indus River basin, which can be attained by incorporating advanced three-dimensional topographic information [162–166], and distributed friction parameters based on vegetation heights [167,168]. Significant advancements and higher accuracy can be further attained in hydrodynamic modeling by treating topographic features explicitly at grid cell scale, and homogeneous features at sub-grid scale [167].

The low-lying areas of the floodplain exhibited good performance compared with the high-lying areas, and reproduced the extreme event successfully. It is recommended that inundation modeling should always be conducted in conjunction with detailed field survey data, for proper validation of results. Probabilistic flood mapping methodologies [145,169], hybrid stochastic approaches [170], and coupled hydrological–hydrodynamic modeling [171] are also recommended to minimize the uncertainties associated with inundation modeling.

5. Conclusions

This hydrodynamic modeling of the central part of the Indus River basin proved to be helpful for indicating the most flood-vulnerable areas. The overall accuracy of the land use map for 2010 and 2015, was 64.06 and 61.64%, with 66 and 73 sampling points, respectively. The calibration (2010) and validation (2015) of the HEC–RAS model resulted in 0.055 and 0.06 optimized n values for the main channels and floodplains, respectively. The model simulation accuracy at optimized n values was reliable. The DSC, F1, and F2, were 0.77, 0.64, and 0.87 for the calibration period, and 0.71, 0.66, and 0.86 for the validation period, respectively. The JD values were 0.23, and 0.19 for the calibration and validation periods, respectively. The increase in simulated flood area was higher, with a small increase in n values of the main channels (rivers), while an increase in the modeled flood area was less, with a higher increase in floodplains' n values. From the results, it can be concluded that HEC–RAS inundation modeling needs proper calibration and validation with in situ flood extent, which may not be possible during a catastrophic flood event. The MODIS and Landsat-based flood extent proved helpful for the comparison of simulated flood extent at different combinations of n values of the main channels and floodplains, and ultimately for the optimization of n values. The reliable results of the calibration and validation periods indicate a good agreement exists between simulated and observed flood extents at most of the places of the floodplains. The HEC–RAS v5 model can be helpful for early flood warning if properly calibrated and validated in the large river basins of the world which have extreme hydrometeorological and complex topographic conditions.

Supplementary Materials: The following supporting information can be downloaded at: <https://www.mdpi.com/article/10.3390/w14192984/s1>, Figure S1: Bands of Landsat 5 Thematic Mapper, Moderate Resolution Imaging Spectroradiometer MOD09A1, MOD09GA, and Landsat 8 Operational Land Imager used in the Analysis; Figure S2: Normalized Difference Water Index (NDWI), Modified Normalized Difference Water Index1, and Modified Normalized Difference Water Index2 used for Flood Mapping.

Author Contributions: Conceptualization, M.A.A., S.A. and A.N.; methodology, M.A.A., A.N. and S.A.; software, M.I.K. and R.A.A.; formal analysis, M.A.A., M.J.M.C. and R.A.A.; investigation, M.M.W., R.A.A. and M.N.; resources, M.I.K., M.M.W. and M.M.; data curation, M.J.M.C., N.S. and A.N.S.; writing—original draft preparation, M.A.A., A.N. and S.A.; writing—review and editing, M.I.K., M.M.W. and M.J.M.C.; visualization, M.N., N.S. and M.M.; supervision, A.N. and A.N.S. All authors have read and agreed to the published version of the manuscript.

Funding: This research has not received any external funding.

Institutional Review Board Statement: Not applicable.

Informed Consent Statement: Not applicable.

Data Availability Statement: Data will be provided on reasonable request.

Conflicts of Interest: The authors declare no conflict of interest.

References

1. Neumayer, E.; Plümpner, T. The gendered nature of natural disasters: The impact of catastrophic events on the gender gap in life expectancy, 1981–2002. *Ann. Assoc. Am. Geogr.* **2007**, *97*, 551–566. [\[CrossRef\]](#)
2. Cannon, T. Vulnerability analysis and the explanation of ‘natural’ disasters. *Disasters Dev. Environ.* **1994**, *1*, 13–30.
3. Ashley, S.T.; Ashley, W.S. Flood fatalities in the United States. *J. Appl. Meteorol. Climatol.* **2008**, *47*, 805–818. [\[CrossRef\]](#)
4. Seyedeh, S.; Thamer, A.; Mahmud, A.; Majid, K.; Amir, S. Integrated Modelling for Flood Hazard Mapping Using Watershed Modelling System. *Am. J. Eng. Appl. Sci.* **2008**, *1*, 149–156.
5. Stefanidis, S.; Stathis, D. Assessment of flood hazard based on natural and anthropogenic factors using analytic hierarchy process (AHP). *Nat. Hazards* **2013**, *68*, 569–585. [\[CrossRef\]](#)
6. Alfieri, L.; Cohen, S.; Galantowicz, J.; Schumann, G.J.; Trigg, M.A.; Zsoter, E.; Prudhomme, C.; Kruczkiewicz, A.; de Perez, E.C.; Flamig, Z.; et al. A global network for operational flood risk reduction. *Environ. Sci.* **2018**, *84*, 149–158. [\[CrossRef\]](#)
7. IRFC. *World Disasters Report, 2003*; International Federation of Red Cross and Red Crescent Societies: Geneva, Switzerland, 2003.
8. ARDC. *Natural Disaster Data Book 2009 (an Analytical Review)*; Asia Disaster Reduction Center: Kobe, Japan, 2009; p. 23.

9. Jongman, B.; Ward, P.J.; Aerts, J.C. Global exposure to river and coastal flooding: Long term trends and changes. *Glob. Environ. Change* **2012**, *22*, 823–835. [\[CrossRef\]](#)
10. Munich, R. *NatCatSERVICE Loss Events Worldwide 1980–2014*; Munich Reinsurance: Munich, Germany, 2015; p. 10.
11. Jonkman, S.N. Global perspectives on loss of human life caused by floods. *Nat. Hazards* **2005**, *34*, 151–175. [\[CrossRef\]](#)
12. Savage, J.T.S.; Bates, P.; Freer, J.; Neal, J.; Aronica, G. When does spatial resolution become spurious in probabilistic flood inundation predictions? *Hydrol. Process.* **2016**, *30*, 2014–2032. [\[CrossRef\]](#)
13. Messner, F.; Meyer, V. Flood damage, vulnerability and risk perception—Challenges for flood damage research. In *Flood Risk Management: Hazards, Vulnerability and Mitigation Measures*; Springer: Dordrecht, The Netherlands, 2006; pp. 149–167.
14. Dutta, D.; Herath, S.; Musiake, K. A mathematical model for flood loss estimation. *J. Hydrol.* **2003**, *277*, 24–49. [\[CrossRef\]](#)
15. Belletti, B.; Dufour, S.; Piégay, H. What is the relative effect of space and time to explain the braided river width and island patterns at a regional scale? *River Res. Appl.* **2015**, *31*, 1–15. [\[CrossRef\]](#)
16. UNESCO. *Water: A Shared Responsibility*; The United Nations World Water Development Report 2, World Water Assessment Programme; UNESCO: Paris, France, 2006.
17. Razavi, S.; Gober, P.; Maier, H.R.; Brouwer, R.; Wheeler, H. Anthropocene flooding: Challenges for science and society. *Hydrol. Process.* **2020**, *34*, 1996–2000. [\[CrossRef\]](#)
18. FFC. *Annual Flood Report, Federal Flood Commission, Ministry of Water and Power of Pakistan*; Water and Power Development Authority: Islamabad, Pakistan, 2017.
19. FFC. *Annual Flood Report, Federal Flood Commission, Ministry of Water and Power of Pakistan*; Water and Power Development Authority: Islamabad, Pakistan, 2018.
20. FFC. *Annual Flood Report, Federal Flood Commission, Ministry of Water and Power of Pakistan*; Water and Power Development Authority: Islamabad, Pakistan, 2020.
21. FFC. *Annual Flood Report, Federal Flood Commission, Ministry of Water and Power of Pakistan*; Water and Power Development Authority: Islamabad, Pakistan, 2014.
22. Archer, D.R.; Forsythe, N.; Fowler, H.J.; Shah, S.M. Sustainability of water resources management in the Indus Basin under changing climatic and socio economic conditions. *Hydrol. Earth Syst. Sci.* **2010**, *14*, 1669–1680. [\[CrossRef\]](#)
23. Biswas, A.K. Indus water treaty: The negotiating process. *Water Int.* **1992**, *17*, 201–209. [\[CrossRef\]](#)
24. Sohail, M.T.; Delin, H.; Siddiq, A. Indus basin waters a main resource of water in Pakistan: An analytical approach. *Curr. World Environ.* **2014**, *9*, 670. [\[CrossRef\]](#)
25. Das, T.; Maurer, E.P.; Pierce, D.W.; Dettinger, M.D.; Cayan, D.R. Increases in flood magnitudes in California under warming climates. *J. Hydrol.* **2013**, *501*, 101–110. [\[CrossRef\]](#)
26. Field, C.B.; Barros, V.; Stocker, T.F.; Dahe, Q. *Managing the Risks of Extreme Events and Disasters to Advance Climate Change Adaptation: Special Report of the Intergovernmental Panel on Climate Change*; Cambridge University Press: Cambridge, UK, 2012.
27. Visser, H.; Petersen, A.C.; Ligtoet, W. On the relation between weather-related disaster impacts, vulnerability and climate change. *Clim. Chang.* **2014**, *125*, 461–477. [\[CrossRef\]](#)
28. Arnell, N.W.; Gosling, S.N. The impacts of climate change on river flood risk at the global scale. *Clim. Chang.* **2016**, *134*, 387–401. [\[CrossRef\]](#)
29. Alfieri, L.; Burek, P.; Feyen, L.; Forzieri, G. Global warming increases the frequency of river floods in Europe. *Hydrol. Earth Syst. Sci.* **2015**, *19*, 2247–2260. [\[CrossRef\]](#)
30. Lehner, B.; Döll, P.; Alcamo, J.; Henrichs, T.; Kaspar, F. Estimating the impact of global change on flood and drought risks in Europe: A continental, integrated analysis. *Clim. Chang.* **2006**, *75*, 273–299. [\[CrossRef\]](#)
31. Plate, E.J. Flood risk and flood management. *J. Hydrol.* **2002**, *267*, 2–11. [\[CrossRef\]](#)
32. Luo, P.; He, B.; Duan, W.; Takara, K.; Nover, D. Impact assessment of rainfall scenarios and land-use change on hydrologic response using synthetic Area IDF curves. *J. Flood Risk Manag.* **2018**, *11*, S84–S97. [\[CrossRef\]](#)
33. Stoffel, M.; Wyzga, B.; Marston, R.A. Floods in mountain environments: A synthesis. *Geomorphology* **2016**, *272*, 1–9. [\[CrossRef\]](#)
34. Krapesch, G.; Hauer, C.; Habersack, H. Scale orientated analysis of river width changes due to extreme flood hazards. *Nat. Hazards Earth Syst. Sci.* **2011**, *11*, 2137–2147. [\[CrossRef\]](#)
35. Dean, D.J.; Schmidt, J.C. The geomorphic effectiveness of a large flood on the Rio Grande in the Big Bend region: Insights on geomorphic controls and post-flood geomorphic response. *Geomorphology* **2013**, *201*, 183–198. [\[CrossRef\]](#)
36. Grove, J.R.; Croke, J.; Thompson, C. Quantifying different riverbank erosion processes during an extreme flood event. *Earth Surf. Process. Landf.* **2013**, *38*, 1393–1406. [\[CrossRef\]](#)
37. Surian, N.; Righini, M.; Lucia, A.; Nardi, L.; Amponsah, W.; Benvenuti, M.; Borga, M.; Cavalli, M.; Comiti, F.; Marchi, L. Channel response to extreme floods: Insights on controlling factors from six mountain rivers in northern Apennines, Italy. *Geomorphology* **2016**, *272*, 78–91. [\[CrossRef\]](#)
38. Fread, D.L. Flow routing. In *Handbook of Hydrology*; McGraw-Hill: New York, NY, USA, 1992; Chapter 10; pp. 316–345.
39. Kundzewicz, Z.W.; Kaczmarek, Z. Coping with hydrological extremes. *Water Int.* **2000**, *25*, 66–75. [\[CrossRef\]](#)
40. Ebert, A.; Kerle, N.; Stein, A. Urban social vulnerability assessment with physical proxies and spatial metrics derived from air-and spaceborne imagery and GIS data. *Nat. Hazards* **2009**, *48*, 275–294. [\[CrossRef\]](#)
41. Ali, S.; Masud Cheema, M.J.; Bakhsh, A.; Khaliq, T. Near real time flood forecasting in the transboundary Chenab river using Global Satellite Mapping of Precipitation. *Pak. J. Agric. Sci.* **2020**, *57*, 1327–1335.

42. Ranzi, R.; Mazzoleni, M.; Milanesi, L.; Pilotti, M.; Ferri, M.; Giuriato, F.; Michel, G.; Fewtrell, T.; Bates, P.D.; Neal, J. Critical review of non-structural measures for water-related risks. In *KULTURisk*; UNESCO-IHE: Delft, The Netherlands, 2011; p. 42.
43. Chiang, P.; Willems, P.; Berlamont, J. A conceptual river model to support real-time flood control (Demer River, Belgium). In Proceedings of the River Flow 2010 International Conference on Fluvial Hydraulics, TU Braunschweig, Braunschweig, Germany, 8–10 September 2010; pp. 8–10.
44. Wu, J.; Liu, H.; Wei, G.; Song, T.; Zhang, C.; Zhou, H. Flash flood forecasting using support vector regression model in a small mountainous catchment. *Water* **2019**, *11*, 1327. [\[CrossRef\]](#)
45. Xiao, Z.; Liang, Z.; Li, B.; Hou, B.; Hu, Y.; Wang, J. New flood early warning and forecasting method based on similarity theory. *J. Hydrol. Eng.* **2019**, *24*, 04019023. [\[CrossRef\]](#)
46. Chu, H.; Wu, W.; Wang, Q.; Nathan, R.; Wei, J. An ANN-based emulation modelling framework for flood inundation modelling: Application, challenges and future directions. *Environ. Model. Softw.* **2020**, *124*, 104587. [\[CrossRef\]](#)
47. Gichamo, T.Z.; Popescu, I.; Jonoski, A.; Solomatine, D. River cross-section extraction from the ASTER global DEM for flood modeling. *Environ. Model. Softw.* **2012**, *31*, 37–46. [\[CrossRef\]](#)
48. Shamaoma, H.; Kerle, N.; Alkema, D. Extraction of flood-modelling related base-data from multi-source remote sensing imagery. In Proceedings of the ISPRS Mid-Term Symposium, Enschede, The Netherlands, 8–11 May 2006.
49. Hunter, N.M.; Bates, P.D.; Horritt, M.S.; Wilson, M.D. Simple spatially-distributed models for predicting flood inundation: A review. *Geomorphology* **2007**, *90*, 208–225. [\[CrossRef\]](#)
50. Horritt, M.; Bates, P. Evaluation of 1D and 2D numerical models for predicting river flood inundation. *J. Hydrol.* **2002**, *268*, 87–99. [\[CrossRef\]](#)
51. Pappenberger, F.; Beven, K.J.; Hunter, N.; Bates, P.; Gouweleeuw, B.; Thielen, J.; De Roo, A. Cascading model uncertainty from medium range weather forecasts (10 days) through a rainfall-runoff model to flood inundation predictions within the European Flood Forecasting System (EFFS). *Hydrol. Earth Syst. Sci. Discuss.* **2005**, *9*, 381–393. [\[CrossRef\]](#)
52. Smirnov, S.; Werner, W. Critical exponents for two-dimensional percolation. *arXiv* **2001**, arXiv:math/0109120v2. [\[CrossRef\]](#)
53. Leon, A.S.; Goodell, C. Controlling hec-ras using matlab. *Environ. Model. Softw.* **2016**, *84*, 339–348. [\[CrossRef\]](#)
54. Dyhouse, G.; Hatchett, J.; Benn, J. *Floodplain Modeling Using HEC-RAS*; Haestad Press: Watertown, CT, USA, 2003.
55. Clark, M.J. Putting water in its place: A perspective on GIS in hydrology and water management. *Hydrol. Process.* **1998**, *12*, 823–834. [\[CrossRef\]](#)
56. Namara, W.G.; Damisse, T.A.; Tufa, F.G. Application of HEC-RAS and HEC-GeoRAS model for Flood Inundation Mapping, the case of Awash Bello Flood Plain, Upper Awash River Basin, Oromiya Regional State, Ethiopia. *Model. Earth Syst. Environ.* **2021**, *8*, 1449–1460. [\[CrossRef\]](#)
57. Maidment, D.R.; Djokic, D. *Hydrologic and Hydraulic Modeling Support: With Geographic Information Systems*; ESRI, Inc.: Redlands, CA, USA, 2000.
58. Samarasinghea, S.; Nandalalb, H.; Welitiyay, D.; Fowzed, J.; Hazarikad, M.; Samarakoond, L. Application of remote sensing and GIS for flood risk analysis: A case study at Kalu-Ganga River, Sri Lanka. *Int. Arch. Photogramm. Remote Sens. Spat. Inf. Sci.* **2010**, *38*, 110–115.
59. Elkhachy, I.; Pham, Q.B.; Costache, R.; Mohajane, M.; Rahman, K.U.; Shahabi, H.; Linh, N.T.T.; Anh, D.T. Sentinel-1 remote sensing data and Hydrologic Engineering Centres River Analysis System two-dimensional integration for flash flood detection and modelling in New Cairo City, Egypt. *J. Flood Risk Manag.* **2021**, *14*, e12692. [\[CrossRef\]](#)
60. Tegos, A.; Ziogas, A.; Bellos, V.; Tzimas, A. Forensic Hydrology: A Complete Reconstruction of an Extreme Flood Event in Data-Scarce Area. *Hydrology* **2022**, *9*, 93. [\[CrossRef\]](#)
61. Ongdas, N.; Akiyanova, F.; Karakulov, Y.; Muratbayeva, A.; Zinabdin, N. Application of HEC-RAS (2D) for flood hazard maps generation for Yesil (Ishim) river in Kazakhstan. *Water* **2020**, *12*, 2672. [\[CrossRef\]](#)
62. Zin, W.W.; Kawasaki, A.; Win, S. River flood inundation mapping in the Bago River Basin, Myanmar. *Hydrol. Res. Lett.* **2015**, *9*, 97–102. [\[CrossRef\]](#)
63. Rahman, M.R.; Thakur, P.K. Detecting, mapping and analysing of flood water propagation using synthetic aperture radar (SAR) satellite data and GIS: A case study from the Kendrapara District of Orissa State of India. *Egypt. J. Remote Sens. Space Sci.* **2018**, *21*, S37–S41. [\[CrossRef\]](#)
64. Liu, Z.; Merwade, V.; Jafarzadegan, K. Investigating the role of model structure and surface roughness in generating flood inundation extents using one-and two-dimensional hydraulic models. *J. Flood Risk Manag.* **2019**, *12*, e12347. [\[CrossRef\]](#)
65. Thomas, H.; Nisbet, T. An assessment of the impact of floodplain woodland on flood flows. *Water Environ. J.* **2007**, *21*, 114–126. [\[CrossRef\]](#)
66. Yalcin, E. Assessing the impact of topography and land cover data resolutions on two-dimensional HEC-RAS hydrodynamic model simulations for urban flood hazard analysis. *Nat. Hazards* **2020**, *101*, 995–1017. [\[CrossRef\]](#)
67. Ali, S.; Cheema, M.J.M.; Waqas, M.M.; Waseem, M.; Awan, U.K.; Khaliq, T. Changes in Snow Cover Dynamics over the Indus Basin: Evidences from 2008 to 2018 MODIS NDSI Trends Analysis. *Remote Sens.* **2020**, *12*, 2782. [\[CrossRef\]](#)
68. Ferrier, K.L.; Mitrovica, J.X.; Giosan, L.; Clift, P.D. Sea-level responses to erosion and deposition of sediment in the Indus River basin and the Arabian Sea. *Earth Planet. Sci. Lett.* **2015**, *416*, 12–20. [\[CrossRef\]](#)
69. Immerzeel, W.W.; Droogers, P.; De Jong, S.; Bierkens, M. Large-scale monitoring of snow cover and runoff simulation in Himalayan river basins using remote sensing. *Remote Sens. Environ.* **2009**, *113*, 40–49. [\[CrossRef\]](#)

70. Immerzeel, W.W.; Van Beek, L.P.; Bierkens, M.F. Climate change will affect the Asian water towers. *Science* **2010**, *328*, 1382–1385. [\[CrossRef\]](#)
71. Tamiru, H.; Dinka, M.O. Application of ANN and HEC-RAS model for flood inundation mapping in lower Baro Akobo River Basin, Ethiopia. *J. Hydrol. Reg. Stud.* **2021**, *36*, 100855. [\[CrossRef\]](#)
72. Vojtek, M.; Petroselli, A.; Vojteková, J.; Asgharinia, S. Flood inundation mapping in small and ungauged basins: Sensitivity analysis using the EBA4SUB and HEC-RAS modeling approach. *Hydrol. Res.* **2019**, *50*, 1002–1019. [\[CrossRef\]](#)
73. Mokhtar, E.S.; Pradhan, B.; Ghazali, A.H.; Shafri, H.Z.M. Assessing flood inundation mapping through estimated discharge using GIS and HEC-RAS model. *Arab. J. Geosci.* **2018**, *11*, 682. [\[CrossRef\]](#)
74. Rangari, V.A.; Umamahesh, N.; Bhatt, C. Assessment of inundation risk in urban floods using HEC RAS 2D. *Model. Earth Syst. Environ.* **2019**, *5*, 1839–1851. [\[CrossRef\]](#)
75. Pradhan, D.; Sahu, R.T.; Verma, M.K. Flood inundation mapping using GIS and Hydraulic model (HEC-RAS): A case study of the Burhi Gandak river, Bihar, India. In *Soft Computing: Theories and Applications*; Springer: Singapore, 2022; pp. 135–145.
76. Marko, K.; Elfeki, A.; Alamri, N.; Chaabani, A. Two dimensional flood inundation modelling in urban areas using WMS, HEC-RAS and GIS (Case Study in Jeddah City, Saudi Arabia). In *Proceedings of the Conference of the Arabian Journal of Geosciences*, Sousse, Tunisia, 12 November 2018; pp. 265–267.
77. Naeem, B.; Azmat, M.; Tao, H.; Ahmad, S.; Khattak, M.U.; Haider, S.; Ahmad, S.; Khoro, Z.; Goodell, C.R. Flood hazard assessment for the tori levee breach of the indus river basin, Pakistan. *Water* **2021**, *13*, 604. [\[CrossRef\]](#)
78. Khalil, U.; Khan, N.M. Assessment of Flood using Geospatial Technique for Indus River Reach: Chashma-Taunsa. *Sci. Int.* **2015**, *27*, 1985–1991.
79. Khattak, M.S.; Anwar, F.; Saeed, T.U.; Sharif, M.; Sheraz, K.; Ahmed, A. Floodplain mapping using HEC-RAS and ArcGIS: A case study of Kabul River. *Arab. J. Sci. Eng.* **2016**, *41*, 1375–1390. [\[CrossRef\]](#)
80. Rind, M.A.; Ansari, K.; Saher, R.; Shakya, S.; Ahmad, S. 2D Hydrodynamic Model for Flood Vulnerability Assessment of Lower Indus River Basin, Pakistan. In *Proceedings of the World Environmental and Water Resources Congress 2018: Watershed Management, Irrigation and Drainage, and Water Resources Planning and Management*, Minneapolis, MN, USA, 3–7 June 2018; pp. 468–482.
81. Abbas Gilany, S.N.; Iqbal, J.; Hussain, E. Geospatial analysis and simulation of glacial lake outburst flood hazard in Hunza and Shyok basins of upper indus basin. *Cryosph. Discuss.* **2020**. *preprint*.
82. Gilany, N.; Iqbal, J. Geospatial analysis and simulation of glacial lake outburst flood hazard in Shyok Basin of Pakistan. *Environ. Earth Sci.* **2020**, *79*, 139. [\[CrossRef\]](#)
83. Shahid, H.; Toyoda, M.; Kato, S. Impact Assessment of Changing Landcover on Flood Risk in the Indus River Basin Using the Rainfall–Runoff–Inundation (RRI). *Sustainability* **2022**, *14*, 7021. [\[CrossRef\]](#)
84. Khalil, U.; Khan, N.M. Floodplain Mapping for Indus River: Chashma–Taunsa Reach. *Pak. J. Eng. Appl. Sci.* **2017**, *20*, 30–48.
85. Werner, M.; van Dijk, M. Developing flood forecasting systems: Examples from the UK, Europe, and Pakistan. In *Proceedings of the International Conference on Innovation Advances and Implementation of Flood Forecasting Technology*, Tromsø, Norway, 17–19 October 2005.
86. Gaurav, K.; Sinha, R.; Panda, P. The Indus flood of 2010 in Pakistan: A perspective analysis using remote sensing data. *Nat. Hazards* **2011**, *59*, 1815–1826. [\[CrossRef\]](#)
87. FFC. *Annual Flood Report, Federal Flood Commission, Ministry of Water and Power of Pakistan*; Water and Power Development Authority: Islamabad, Pakistan, 2010.
88. Amarnath, G.; Rajah, A. An evaluation of flood inundation mapping from MODIS and ALOS satellites for Pakistan. *Geomat. Nat. Hazards Risk* **2016**, *7*, 1526–1537. [\[CrossRef\]](#)
89. Qazi, S.; Alam, S.; Piracha, S. The prevalence of major depression in a rural flood affected area of Pakistan. *Pak. J. Med. Health Sci.* **2014**, *8*, 249–252.
90. Aslam, N.; Kamal, A. Stress, anxiety, depression, and posttraumatic stress disorder among general population affected by floods in Pakistan. *Pak. J. Med. Res.* **2016**, *55*, 29.
91. Chung, M.C.; Jalal, S.; Khan, N.U. Posttraumatic stress disorder and psychiatric comorbidity following the 2010 flood in Pakistan: Exposure characteristics, cognitive distortions, and emotional suppression. *Psychiatry* **2014**, *77*, 289–304. [\[CrossRef\]](#)
92. Fatima, N.; Rana, S. Repercussion of Flood of 2010 on the Mental Health of Pakistani Victims. *Pak. J. Soc. Clin. Psychol.* **2017**, *15*, 42–52.
93. Sitwat, A.; Asad, S.; Yousaf, A. Psychopathology, psychiatric symptoms and their demographic correlates in female adolescents flood victims. *J. Coll. Physicians Surg. Pak.* **2015**, *25*, 886–890. [\[PubMed\]](#)
94. Afzal, M.; Sultan, M. Experience of malaria in children of a flood affected area: A field hospital study. *East. Mediterr. Health J.* **2013**, *19*, 613–616. [\[CrossRef\]](#)
95. Afzal, M.N.; Rana, S.A.; Farooq, M.; Qureshi, I.H. Malaria in Adults Presenting with Fever in Flood Affected Region of Southern Punjab, Pakistan. *Infect. Dis. J. Pak.* **2012**, *21*, 402–403.
96. Warraich, H.; Zaidi, A.K.; Patel, K. Floods in Pakistan: A public health crisis. *Bull. World Health Organ.* **2011**, *89*, 236–237. [\[CrossRef\]](#) [\[PubMed\]](#)
97. Mallett, L.H.; Etzel, R.A. Flooding: What is the impact on pregnancy and child health? *Disasters* **2018**, *42*, 432–458. [\[CrossRef\]](#)

98. Tariq, M.A.U.R.; Van De Giesen, N. Floods and flood management in Pakistan. *Phys. Chem. Earth Parts A B C* **2012**, *47*, 11–20. [[CrossRef](#)]
99. FFC. *Annual Flood Report, Federal Flood Commission, Ministry of Water and Power of Pakistan*; Water and Power Development Authority: Islamabad, Pakistan, 2015.
100. Sayed, S.A.; González, P.A. Flood disaster profile of Pakistan: A review. *Sci. J. Public Health* **2014**, *2*, 144–149. [[CrossRef](#)]
101. Ahmed, K.; Shahbaz, M.; Qasim, A.; Long, W. The linkages between deforestation, energy and growth for environmental degradation in Pakistan. *Ecol. Indic.* **2015**, *49*, 95–103. [[CrossRef](#)]
102. Oxley, M. Field note from Pakistan floods: Preventing future flood disasters. *J. Disaster Risk Stud.* **2011**, *3*, 453–461. [[CrossRef](#)]
103. Saeed, T.U.; Attaullah, H. Impact of extreme floods on groundwater quality (in Pakistan). *Br. J. Environ. Clim. Chang.* **2014**, *4*, 133. [[CrossRef](#)]
104. Raza, M.; Hussain, F.; Lee, J.-Y.; Shakoor, M.B.; Kwon, K.D. Groundwater status in Pakistan: A review of contamination, health risks, and potential needs. *Crit. Rev. Environ. Sci. Technol.* **2017**, *47*, 1713–1762. [[CrossRef](#)]
105. Ullah, S.; Javed, M.W.; Rasheed, S.B.; Jamal, Q.; Aziz, F.; Ullah, S. Assessment of groundwater quality of district Dir Lower Pakistan. *Int. J. Biosci.* **2014**, *4*, 248–255.
106. Mahmood, S.; Rahman, A.-U.; Sajjad, A. Assessment of 2010 flood disaster causes and damages in district Muzaffargarh, Central Indus Basin, Pakistan. *Environ. Earth Sci.* **2019**, *78*, 63. [[CrossRef](#)]
107. Hashim, N.H.; Qazi, T.M.S.; Abdul, R.G.; Mumtaz, A.K.; Habib, U.R.M. A critical analysis of 2010 floods in Pakistan. *Afr. J. Agric. Res.* **2012**, *7*, 1054–1067.
108. Wolf, A.T.; Natharius, J.A.; Danielson, J.J.; Ward, B.S.; Pender, J.K. International river basins of the world. *Int. J. Water Resour. Dev.* **1999**, *15*, 387–427. [[CrossRef](#)]
109. Lutz, A.F.; ter Maat, H.W.; Biemans, H.; Shrestha, A.B.; Wester, P.; Immerzeel, W.W. Selecting representative climate models for climate change impact studies: An advanced envelope-based selection approach. *Int. J. Climatol.* **2016**, *36*, 3988–4005. [[CrossRef](#)]
110. Bajracharya, S.R.; Shrestha, B.R. *The Status of Glaciers in the Hindu Kush-Himalayan Region*; International Centre for Integrated Mountain Development (ICIMOD): Kathmandu, Nepal, 2011.
111. Ali, A. *Indus Basin Floods: Mechanisms, Impacts, and Management*; Asian Development Bank: Mandaluyong City, Philippines, 2013.
112. Ramly, S.; Tahir, W.; Abdullah, J.; Jani, J.; Ramli, S.; Asmat, A. Flood Estimation for SMART Control Operation Using Integrated Radar Rainfall Input with the HEC-HMS Model. *Water Resour. Manag.* **2020**, *34*, 3113–3127. [[CrossRef](#)]
113. Natarajan, S.; Radhakrishnan, N. An Integrated Hydrologic and Hydraulic Flood Modeling Study for a Medium-Sized Ungauged Urban Catchment Area: A Case Study of Tiruchirappalli City Using HEC-HMS and HEC-RAS. *J. Inst. Eng. Ser. A* **2020**, *101*, 381–398. [[CrossRef](#)]
114. Cho, Y. Application of NEXRAD Radar-Based Quantitative Precipitation Estimations for Hydrologic Simulation Using ArcPy and HEC Software. *Water* **2020**, *12*, 273. [[CrossRef](#)]
115. Teng, F.; Huang, W.; Ginis, I. Hydrological modeling of storm runoff and snowmelt in Taunton River Basin by applications of HEC-HMS and PRMS models. *Nat. Hazards* **2018**, *91*, 179–199. [[CrossRef](#)]
116. Tucker, C.J. Red and photographic infrared linear combinations for monitoring vegetation. *Remote Sens. Environ.* **1979**, *8*, 127–150. [[CrossRef](#)]
117. Arcement, G.J.; Schneider, V.R. *Guide for Selecting Manning's Roughness Coefficients for Natural Channels and Flood Plains*; Department of the Interior, US Geological Survey: Reston, VA, USA, 1989.
118. Jobe, A.; Kalra, A.; Ibendahl, E. Conservation Reserve Program effects on floodplain land cover management. *J. Environ. Manag.* **2018**, *214*, 305–314. [[CrossRef](#)] [[PubMed](#)]
119. Fischer, G.; Nachtergaele, F.; Prieler, S.; Van Velthuisen, H.; Verelst, L.; Wiberg, D. *Global Agro-Ecological Zones Assessment for Agriculture (GAEZ 2008)*; IASA: Laxenburg, Austria; FAO: Rome, Italy, 2008; p. 10.
120. Srivastava, P.K.; Han, D.; Rico-Ramirez, M.A.; O'Neill, P.; Islam, T.; Gupta, M. Assessment of SMOS soil moisture retrieval parameters using tau-omega algorithms for soil moisture deficit estimation. *J. Hydrol.* **2014**, *519*, 574–587. [[CrossRef](#)]
121. Yang, D.; Gao, B.; Jiao, Y.; Lei, H.; Zhang, Y.; Yang, H.; Cong, Z. A distributed scheme developed for eco-hydrological modeling in the upper Heihe River. *Sci. China Earth Sci.* **2015**, *58*, 36–45. [[CrossRef](#)]
122. Nicholas, A.; Mitchell, C. Numerical simulation of overbank processes in topographically complex floodplain environments. *Hydrol. Process.* **2003**, *17*, 727–746. [[CrossRef](#)]
123. Horritt, M.; Bates, P. Effects of spatial resolution on a raster based model of flood flow. *J. Hydrol.* **2001**, *253*, 239–249. [[CrossRef](#)]
124. Logan, T.A.; Nicoll, J.; Laurencelle, J.; Hogenson, K.; Gens, R.; Buechler, B.; Barton, B.; Shreve, W.; Stern, T.; Drew, L. Radiometrically terrain corrected ALOS PALSAR Data available from the Alaska Satellite Facility. In Proceedings of the AGU Fall Meeting Abstracts, San Francisco, CA, USA, 13–17 December 2014; p. IN33B-3762.
125. Loew, A.; Mauser, W. Generation of geometrically and radiometrically terrain corrected SAR image products. *Remote Sens. Environ.* **2007**, *106*, 337–349. [[CrossRef](#)]
126. Brunner, G.W. *HEC-RAS River Analysis System 2D Modeling User's Manual*; US Army Corps of Engineers—Hydrologic Engineering Center: Davis, CA, USA, 2016; pp. 1–171.
127. Quiroga, V.M.; Kurea, S.; Udoa, K.; Manoa, A. Application of 2D numerical simulation for the analysis of the February 2014 Bolivian Amazonia flood: Application of the new HEC-RAS version 5. *Ribagua* **2016**, *3*, 25–33. [[CrossRef](#)]

128. McFeeters, S.K. The use of the Normalized Difference Water Index (NDWI) in the delineation of open water features. *Int. J. Remote Sens.* **1996**, *17*, 1425–1432. [[CrossRef](#)]
129. Xu, H. Modification of normalised difference water index (NDWI) to enhance open water features in remotely sensed imagery. *Int. J. Remote Sens.* **2006**, *27*, 3025–3033. [[CrossRef](#)]
130. Ji, L.; Zhang, L.; Wylie, B. Analysis of dynamic thresholds for the normalized difference water index. *Photogramm. Eng. Remote Sens.* **2009**, *75*, 1307–1317. [[CrossRef](#)]
131. Lu, S.; Wu, B.; Yan, N.; Wang, H. Water body mapping method with HJ-1A/B satellite imagery. *Int. J. Appl. Earth Obs. Geoinf.* **2011**, *13*, 428–434. [[CrossRef](#)]
132. Gao, B.C. NDWI—A normalized difference water index for remote sensing of vegetation liquid water from space. *Remote Sens. Environ.* **1996**, *58*, 257–266. [[CrossRef](#)]
133. Li, W.; Du, Z.; Ling, F.; Zhou, D.; Wang, H.; Gui, Y.; Sun, B.; Zhang, X. A comparison of land surface water mapping using the normalized difference water index from TM, ETM+ and ALI. *Remote Sens.* **2013**, *5*, 5530–5549. [[CrossRef](#)]
134. Chen, F.; Chen, X.; Van de Voorde, T.; Roberts, D.; Jiang, H.; Xu, W. Open water detection in urban environments using high spatial resolution remote sensing imagery. *Remote Sens. Environ.* **2020**, *242*, 111706. [[CrossRef](#)]
135. Hui, F.; Xu, B.; Huang, H.; Yu, Q.; Gong, P. Modelling spatial-temporal change of Poyang Lake using multitemporal Landsat imagery. *Int. J. Remote Sens.* **2008**, *29*, 5767–5784. [[CrossRef](#)]
136. Feng, L.; Hu, C.; Chen, X.; Cai, X.; Tian, L.; Gan, W. Assessment of inundation changes of Poyang Lake using MODIS observations between 2000 and 2010. *Remote Sens. Environ.* **2012**, *121*, 80–92. [[CrossRef](#)]
137. Rokni, K.; Ahmad, A.; Selamat, A.; Hazini, S. Water feature extraction and change detection using multitemporal Landsat imagery. *Remote Sens.* **2014**, *6*, 4173–4189. [[CrossRef](#)]
138. Du, Z.; Bin, L.; Ling, F.; Li, W.; Tian, W.; Wang, H.; Gui, Y.; Sun, B.; Zhang, X. Estimating surface water area changes using time-series Landsat data in the Qingjiang River Basin, China. *J. Appl. Remote Sens.* **2012**, *6*, 063609. [[CrossRef](#)]
139. Yan, D.; Huang, C.; Ma, N.; Zhang, Y. Improved Landsat-Based Water and Snow Indices for Extracting Lake and Snow Cover/Glacier in the Tibetan Plateau. *Water* **2020**, *12*, 1339. [[CrossRef](#)]
140. Du, Z.; Li, W.; Zhou, D.; Tian, L.; Ling, F.; Wang, H.; Gui, Y.; Sun, B. Analysis of Landsat-8 OLI imagery for land surface water mapping. *Remote Sens. Lett.* **2014**, *5*, 672–681. [[CrossRef](#)]
141. Panteras, G.; Cervone, G. Enhancing the temporal resolution of satellite-based flood extent generation using crowdsourced data for disaster monitoring. *Int. J. Remote Sens.* **2018**, *39*, 1459–1474. [[CrossRef](#)]
142. Sharma, R.C.; Tateishi, R.; Hara, K.; Nguyen, L.V. Developing superfine water index (SWI) for global water cover mapping using MODIS data. *Remote Sens.* **2015**, *7*, 13807–13841. [[CrossRef](#)]
143. Baig, M.H.A.; Zhang, L.; Wang, S.; Jiang, G.; Lu, S.; Tong, Q. Comparison of MNDWI and DFI for water mapping in flooding season. In Proceedings of the 2013 IEEE International Geoscience and Remote Sensing Symposium—IGARSS, Melbourne, VIC, Australia, 21–26 July 2013; pp. 2876–2879.
144. Ogilvie, A.; Belaud, G.; Delenne, C.; Bailly, J.-S.; Bader, J.-C.; Oleksiak, A.; Ferry, L.; Martin, D. Decadal monitoring of the Niger Inner Delta flood dynamics using MODIS optical data. *J. Hydrol.* **2015**, *523*, 368–383. [[CrossRef](#)]
145. Dimitriadis, P.; Tegos, A.; Oikonomou, A.; Pagana, V.; Koukouvinos, A.; Mamassis, N.; Koutsoyiannis, D.; Efstratiadis, A. Comparative evaluation of 1D and quasi-2D hydraulic models based on benchmark and real-world applications for uncertainty assessment in flood mapping. *J. Hydrol.* **2016**, *534*, 478–492. [[CrossRef](#)]
146. Di Baldassarre, G.; Schumann, G.; Bates, P.D. A technique for the calibration of hydraulic models using uncertain satellite observations of flood extent. *J. Hydrol.* **2009**, *367*, 276–282. [[CrossRef](#)]
147. Horritt, M.; Di Baldassarre, G.; Bates, P.; Brath, A. Comparing the performance of a 2-D finite element and a 2-D finite volume model of floodplain inundation using airborne SAR imagery. *Hydrol. Process. Int. J.* **2007**, *21*, 2745–2759. [[CrossRef](#)]
148. Kouwen, N.; Fathi-Moghadam, M. Nonrigid, nonsubmerged, vegetative roughness on floodplains. *J. Hydraul. Eng.* **1997**, *123*, 51–57.
149. Werner, M.; Hunter, N.; Bates, P. Identifiability of distributed floodplain roughness values in flood extent estimation. *J. Hydrol.* **2005**, *314*, 139–157. [[CrossRef](#)]
150. Saksena, S.; Merwade, V. Incorporating the effect of DEM resolution and accuracy for improved flood inundation mapping. *J. Hydrol.* **2015**, *530*, 180–194. [[CrossRef](#)]
151. Karamouz, M.; Mahani, F.F. DEM uncertainty based coastal flood inundation modeling considering water quality impacts. *Water Resour. Manag.* **2021**, *35*, 3083–3103. [[CrossRef](#)]
152. Cook, A.; Merwade, V. Effect of topographic data, geometric configuration and modeling approach on flood inundation mapping. *J. Hydrol.* **2009**, *377*, 131–142. [[CrossRef](#)]
153. Erpicum, S.; Dewals, B.; Archambeau, P.; Detrembleur, S.; Piroton, M. Detailed inundation modelling using high resolution DEMs. *Eng. Appl. Comput. Fluid Mech.* **2010**, *4*, 196–208. [[CrossRef](#)]
154. Baldwin, D.S.; Rees, G.N.; Wilson, J.S.; Colloff, M.J.; Whitworth, K.L.; Pitman, T.L.; Wallace, T.A. Provisioning of bioavailable carbon between the wet and dry phases in a semi-arid floodplain. *Oecologia* **2013**, *172*, 539–550. [[CrossRef](#)]
155. Alsdorf, D.E.; Rodríguez, E.; Lettenmaier, D.P. Measuring surface water from space. *Rev. Geophys.* **2007**, *45*, 1–24. [[CrossRef](#)]
156. Clement, M.A.; Kilsby, C.; Moore, P. Multi-temporal synthetic aperture radar flood mapping using change detection. *J. Flood Risk Manag.* **2018**, *11*, 152–168. [[CrossRef](#)]

157. Anusha, N.; Bharathi, B. Flood detection and flood mapping using multi-temporal synthetic aperture radar and optical data. *Egypt. J. Remote Sens. Space Sci.* **2020**, *23*, 207–219. [[CrossRef](#)]
158. Pedrozo-Acuña, A.; Rodríguez-Rincón, J.P.; Arganis-Juárez, M.; Domínguez-Mora, R.; González Villareal, F.J. Estimation of probabilistic flood inundation maps for an extreme event: Pánuco River, México. *J. Flood Risk Manag.* **2015**, *8*, 177–192. [[CrossRef](#)]
159. Horritt, M.S. Calibration of a two-dimensional finite element flood flow model using satellite radar imagery. *Water Resour. Res.* **2000**, *36*, 3279–3291. [[CrossRef](#)]
160. Horritt, M. Evaluating wetting and drying algorithms for finite element models of shallow water flow. *Int. J. Numer. Methods Eng.* **2002**, *55*, 835–851. [[CrossRef](#)]
161. Oberstadler, R.; Hönsch, H.; Huth, D. Assessment of the mapping capabilities of ERS-1 SAR data for flood mapping: A case study in Germany. *Hydrol. Process.* **1997**, *11*, 1415–1425. [[CrossRef](#)]
162. Patel, D.P.; Ramirez, J.A.; Srivastava, P.K.; Bray, M.; Han, D. Assessment of flood inundation mapping of Surat city by coupled 1D/2D hydrodynamic modeling: A case application of the new HEC-RAS 5. *Nat. Hazards* **2017**, *89*, 93–130. [[CrossRef](#)]
163. Vozinaki, A.-E.K.; Morianou, G.G.; Alexakis, D.D.; Tsanis, I.K. Comparing 1D and combined 1D/2D hydraulic simulations using high-resolution topographic data: A case study of the Koiliaris basin, Greece. *Hydrol. Sci. J.* **2017**, *62*, 642–656. [[CrossRef](#)]
164. Sarchani, S.; Seiradakis, K.; Coulibaly, P.; Tsanis, I. Flood inundation mapping in an ungauged basin. *Water* **2020**, *12*, 1532. [[CrossRef](#)]
165. Noh, S.J.; Lee, J.-H.; Lee, S.; Kawaike, K.; Seo, D.-J. Hyper-resolution 1D-2D urban flood modelling using LiDAR data and hybrid parallelization. *Environ. Model. Softw.* **2018**, *103*, 131–145. [[CrossRef](#)]
166. Jamali, B.; Löwe, R.; Bach, P.M.; Urich, C.; Arnbjerg-Nielsen, K.; Deletic, A. A rapid urban flood inundation and damage assessment model. *J. Hydrol.* **2018**, *564*, 1085–1098. [[CrossRef](#)]
167. Mason, D.C.; Cobby, D.M.; Horritt, M.S.; Bates, P.D. Floodplain friction parameterization in two-dimensional river flood models using vegetation heights derived from airborne scanning laser altimetry. *Hydrol. Process.* **2003**, *17*, 1711–1732. [[CrossRef](#)]
168. Horritt, M. Development of physically based meshes for two-dimensional models of meandering channel flow. *Int. J. Numer. Methods Eng.* **2000**, *47*, 2019–2037. [[CrossRef](#)]
169. Dimitriadis, P.; Tegos, A.; Petsiou, A.; Pagana, V.; Apostolopoulos, I.; Vassilopoulos, E.; Gini, M.; Koussis, A.; Mamassis, N.; Koutsoyiannis, D. Flood Directive implementation in Greece: Experiences and future improvements. *Eur. Water* **2017**, *57*, 35–41.
170. Efstratiadis, A.; Dimas, P.; Pouliasis, G.; Tsoukalas, I.; Kossieris, P.; Bellos, V.; Sakki, G.-K.; Makropoulos, C.; Michas, S. Revisiting Flood Hazard Assessment Practices under a Hybrid Stochastic Simulation Framework. *Water* **2022**, *14*, 457. [[CrossRef](#)]
171. Bellos, V.; Tsakiris, G. A hybrid method for flood simulation in small catchments combining hydrodynamic and hydrological techniques. *J. Hydrol.* **2016**, *540*, 331–339. [[CrossRef](#)]